NJC

Accepted Manuscript

This is an *Accepted Manuscript*, which has been through the Royal Society of Chemistry peer review process and has been accepted for publication.

Accepted Manuscripts are published online shortly after acceptance, before technical editing, formatting and proof reading. Using this free service, authors can make their results available to the community, in citable form, before we publish the edited article. We will replace this *Accepted Manuscript* with the edited and formatted *Advance Article* as soon as it is available.

You can find more information about *Accepted Manuscripts* in the Information for Authors.

Please note that technical editing may introduce minor changes to the text and/or graphics, which may alter content. The journal's standard Terms & Conditions and the Ethical guidelines still apply. In no event shall the Royal Society of Chemistry be held responsible for any errors or omissions in this *Accepted Manuscript* or any consequences arising from the use of any information it contains.

ROYAL SOCIETY OF CHEMISTRY

www.rsc.org/njc

A Terbium Rich Orthoborate $LiSrTb_2(BO_3)_3$ and its analogues

Pengyun Chen,[a,b] Mingjun Xia [a], R. K. Li*[a]

A terbium rich orthoborate, $LiSrTb_2(BO_3)_3$ has been successfully synthesized by solid state reaction and crystallized from high temperature flux. Single crystal X-ray diffraction results show that $LiSrTb_2(BO_3)_3$ possesses $P\bar{3}m1$ space group, with cell parameters of a = 10.3845(4) Å, c = 6.4739(8) Å, and Z =3. In the structure, the terbium atom coordinates to eight oxygen atoms to yield a TbO_8 polyhedron. Those polyhedra are connected with each other to form a layer of trigonal $[Tb_3O_{21}]$ and hexagonal $[Tb_6O_{33}]$ blocks in the *ab* plane, and then the layers are further linked by the triangular BO_3 groups along the *c* direction. The magnetic susceptibility measurements show that $LiSrTb_2(BO_3)_3$ exhibits paramagnetic behaviors from 2 K to 300 K. The diffuse optical reflection spectrum indicates that $LiSrTb_2(BO_3)_3$ is transparent in the range of 500–1500 nm, and effective green emission is detected in the photoluminescence of $LiSrTb_2(BO_3)_3$. In addition, a series of isostructural lanthanide analogues $LiSrLn_2(BO_3)_3$ (Ln=Pr, Nd, Sm-Lu) and $LiBaLn_2(BO_3)_3$ (Ln=Pr, Nd, Sm-Tm) have also been prepared by solid state reaction.

Introduction

Trivalent terbium-based materials have been of various interests in the past several years due to their diverse magnetic and optical applications. The well-known terbium gallium garnet $Tb_3Ga_5O_{12}$ (TGG), with a high terbium concentration and cubic symmetry, has been commercially utilized as magnetic-optical (MO) materials in optical isolators.[1-2] Recently, several terbium-rich compounds with uniaxial or cubic space groups have been explored as MO materials, such as $Tb_3[Sc_{2-x}Lu_x]Al_3O_{12}$, Tb_2O_3, $Tb_{4.67}Si_3O_{13}$, and $LiTbF_4$.[3-6] Besides, substantial attentions have been paid to the Tb^{3+}-doped materials, which have great application prospects in plasma display panels (PDP) and in biochemical probes due to their brilliant green fluorescence as well as high chemical stability.[7-8]

Inorganic borates have been continuously investigated in modern laser technology owing to their excellent transparency and abundant structure types.[9] In order to explore new functional materials, considerable efforts have been focused on the Ln_2O_3-B_2O_3 systems (Ln= lanthanide). TbB_5O_9 has been found to be a good green-emitting UV-LED phosphor for effective energy transfer and absence of concentration quenching.[10] Although several borates with rich terbium contents were reported on the A_2O-Ln_2O_3-B_2O_3 systems (A= alkali-metal), unfortunately most of them could not serve as MO material candidates owing to the low symmetry.[11-12] Among the AEO-Ln_2O_3-B_2O_3 systems (AE= alkaline earth), $Sr_3Tb(BO_3)_3$, with $R\bar{3}$ space group, has been reported as MO materials with the excellent transparency in the visible region despite the pale terbium content.[13] Recently, we are interested in searching new materials in the Li_2O-AEO-Ln_2O_3-B_2O_3 quaternary systems, although previously few reports, such as $Sr_2ScLiB_4O_{10}$, $LiSrY_2(BO_3)_3$, $LiSr_3La_4(BO_3)_6$, on this system have been published,[14-16] in order to search a terbium-based borate that possesses a rich terbium content and uniaxial symmetry at the same time. In this paper, we report the structure, synthesis, optical and magnetic properties of a terbium rich trigonal orthoborate $LiSrTb_2(BO_3)_3$, isostructural to $LiSrY_2(BO_3)_3$[15], as well as its analogues $LiMLn_2(BO_3)_3$ (M=Sr, Ln=Pr, Nd, Sm-Lu; M=Ba, Ln=Pr, Nd, Sm-Tm).

Experimental Section

Solid-State Syntheses

All of the reagents (H_3BO_3, $SrCO_3$, $BaCO_3$, Li_2CO_3, Tb_4O_7, Pr_6O_{11} and Ln_2O_3 for Nd, Sm-Lu) are analytical pure from Shanghai Reagent Factory (Shanghai, China).

Polycrystalline samples of $LiMLn_2(BO_3)_3$ were prepared by solid-state reaction at high-temperature. Stoichiometric mixtures of Li_2CO_3, $SrCO_3$, $BaCO_3$, R_2O_3 and H_3BO_3 were put into the alumina crucibles and heated at 500°C, 700°C, and 800°C with several thorough grindings. 5 % excess molar ratio of $LiBO_2$ was added into the samples during the sintering to compensate the loss for the volatilization of Li_2CO_3 and H_3BO_3. The mixtures were repeatedly sintered at 800 °C with intermediate grindings until the samples did not show any variations in powder X-ray diffraction patterns.

Crystal Growth of $LiSrTb_2(BO_3)_3$

Raw materials were weighed according to the molar ratio of Tb_4O_7: $SrCO_3$: H_3BO_3: Li_2CO_3 =1:12:12:6.

The starting chemicals were ground, mixed and feed into a Pt crucible. The Pt crucible was transported into a resistance heating furnace, which was gradually raised to 950 °C with a heating rate of 50 °C /h and held at this temperature for 24 h for homogenizing. Then, the high-temperature solution was cooled at a rate of 1.5 °C /h to 500 °C. After that, the furnace was turned off and cooled down to room temperature. Colorless transparent crystals in millimeter sizes were obtained after washed by deionized water and ethanol.

Characterizations

Single crystal of $LiSrTb_2(BO_3)_3$ with dimensions of 0.08 × 0.08 × 0.05 mm^3 was selected for the structure determination. Single crystal X-ray diffraction data were collected on a Rigaku XtaLAB-mini diffractometer with a graphite-monochromatized Mo Ka radiation (λ= 0.71073 Å) at room temperature. The SHELXS and SHELXL packages were applied to solve and refine the structures of the crystal. [17]

Powder X-ray diffraction (PXRD) patterns were recorded on a Bruker D8 X-ray diffractometer with a Cu Kα radiation (λ= 1.5418 Å) at room temperature in 2θ range from 10° to 70° with a step size of 0.1°.

The element content in the compounds was determined using the Varian 710-ES inductively coupled plasma -atomic emission spectrometry (ICP-AES).

UV–Vis–NIR diffuse optical reflection spectrum of the title compound was recorded with a Cary 5000 UV–visible–near IR spectrophotometer in the wavelength range from 200 to 2500 nm. Fluoride resin was applied as the standard substance.

Infrared (IR) spectrum was recorded on the Excalibur 3100 with an infrared spectrophotometer in the range of 400-4000 cm^{-1} using KBr pellets. Raman spectrum was taken on an inVia-Reflex micro-zone Raman spectrometer from 400 to 4000 cm^{-1}. Room-temperature photoluminescence was performed on an Edinburgh F900 fluorescence spectrometer.

The usual measurements of magnetic susceptibility against temperature and magnetization against field were carried out in the temperature range 2-300 K at 500 Oe field and up to 9T at 2K, respectively, using a vibrating sample magnetometer (VSM) in Physical Property Measurement System (PPMS-9, Quantum Design).

Differential scanning calorimetry (DSC) was investigated by a Labsys TMTG-DTA16 (SETARAM) in N_2 atmosphere at 10 °C/min heating rate with Al_2O_3 as reference.

Results and Discussion

Crystal Structure

According to the systematic absence from single crystal X-ray diffraction data, *P*3, $P\bar{3}$ and $P\bar{3}$m1 space group were suggested by the XPREP program.[18] All of them were applied for solving the structure and $P\bar{3}$m1 was recommended by PLATON program[19] after the structure solutions were found. Finally, $LiSrTb_2(BO_3)_3$ was refined with the space group $P\bar{3}$m1 and the unit cell parameters of a = 10.3845(9) Å, c = 6.4739(8) Å, and Z =3. The chemical composition $LiSrTb_2(BO_3)_3$ obtained by the structure solution is in good accordance with the ICP-AES analysis results of Sr: Li: Tb: B= 1: 1.2: 2.1: 3.3. The detailed crystallographic data are listed in Table 1. Final atomic coordinates, site occupancy factors (SOF) and equivalent isotropic displacement parameters are summarized in Table 2; selected bond distances are given in Table 3.

Table 1. Crystallographic data of $LiSrTb_2(BO_3)_3$

Formula	$LiSrTb_2(BO_3)_3$
M	588.83
Temperature/K	298(2)
Crystal system	trigonal
Space group	$P\bar{3}$m1
a/Å	10.3845(9)
c/Å	6.4739(8)
cell vol/$Å^3$	604.60(13)
Z	3
Absorption coefficient (mm^{-1})	23.974
GOF	1.147
R1(all reflns)	0.0378
R1($I \geq 2\delta(I)$)	0.0311
wR2 (all reflns)	0.0732
wR2 ($I \geq 2\delta(I)$)	0.0704

Table 2 Atomic coordinates, SOF and equivalent isotropic temperature factors for $LiSrTb_2(BO_3)_3$

Atoms	Wyckoff.	S.O.F.	x	y	z	U_{eq}	BVS
Tb	6i	1	0.17709(3)	0.82291(3)	0.35818(8)	0.0123 (2)	2.972
Sr	3e	1	0	1/2	0	0.0086(3)	1.96
O1	6i	1	0.1796(8)	0.5898(4)	0.3332(10)	0.0089(15)	
O2	12j	1	0.6260(8)	-0.3014(7)	0.6906(8)	0.0192(13)	
O3	6i	1	0.1978(5)	0.8022(5)	0.0100(11)	0.019(2)	
O4	6h	1/2	0.124(2)	0.124(2)	1/2	0.069(8)	
B1	2d	1	1/3	2/3	0.331(3)	0.009(4)	2.913
B2	6i	1	0.1896(8)	0.8104(8)	-0.1965(18)	0.013(3)	2.947
B3	1b	1	0	0	1/2	0.068(17)	3.816
Li	3f	1	0	1/2	1/2	0.030(8)	1.118

There are ten crystallograpically independent atoms, namely Tb, Sr, O(1), O(2), O(3), O(4), B(1), B(2), B(3) and Li, in the unit cell of $LiSrTb_2(BO_3)_3$ (Table 2). It can be seen that Sr, O(4), B(1), B(3) and Li are located at special sites, and all atoms are fully occupied except O(4) with half occupancy. Tb atom coordinates with eight oxygen atoms forming a TbO_8 polyhedron where the distances between the Tb atoms and the oxygen atoms range from 2.28 to 2.46 Å in good agreement with literature values. As shown in Figure 1a, six TbO_8 polyhedra are interconnected by edge- or face-sharing to produce a hexagonal $[Tb_6O_{33}]$ block along the *c*-axis. The $[Tb_6O_{33}]$ block is corner-shared with the adjacent blocks to form a two-dimensional layer parallel to the *ab* plane. In the $[Tb_6O_{33}]_n$ layer, three sorts of tunnels are present as trigonal, hexagonal, and rhombic. The trigonal and hexagonal tunnels are occupied by the triangle $B(1)O_3$ and $B(3)O_3$ groups, respectively, and the rhombic tunnels accommodate with the distorted LiO_6 octahedra. Therefore, the construction of the Tb_6O_{33} layer is reinforced by the connections with the $B(1)O_3$, $B(3)O_3$, and LiO_6 groups. These layers are further bridged by triangular $B(2)O_3$ groups in the third dimension (Figure 1b). Meanwhile, Sr atoms, situated in the interstices between these polyhedral layers, are surrounded by ten oxygen atoms and serve as stitches to support the connection of the layers.

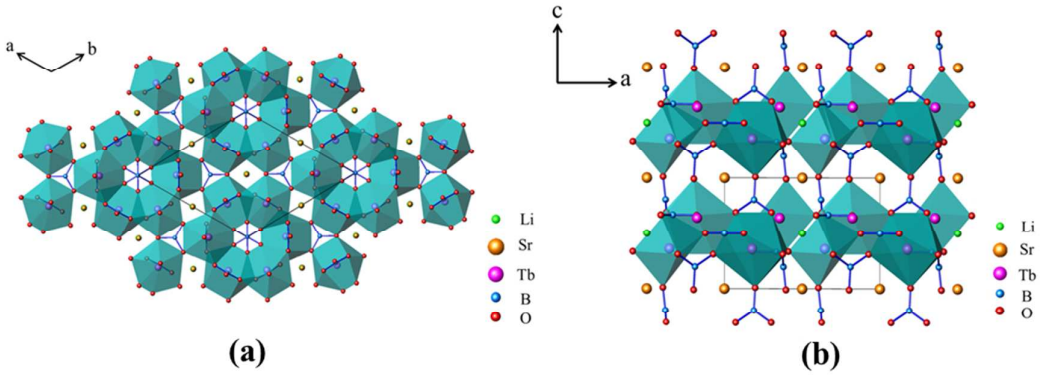

Figure 1. Crystal structure of $LiSrTb_2(BO_3)_3$ along the *c*-axis (a) and along the *b* direction (b)

Table 3. Selected bond lengths (Å) of $LiSrTb_2(BO_3)_3$

Tb-O1 × 2	2.439(5)	B1-O1 × 3	1.382(7)
Tb-O2 × 2	2.464(5)	B2-O2 × 2	1.395(8)
Tb-O2 × 2	2.388(6)	B2-O3	1.345(13)
Tb-O3	2.285(8)	B3-O4 × 3	1.28(2)
Tb-O4	2.357(15)	Sr-O1× 2	2.695(7)
Li-O1× 2	1.943(7)	Sr-O2 × 4	2.698(6)
Li-O2 × 4	2.188(6)	Sr-O3 × 4	2.761(3)

It is worthwhile to note that the bond length (1.287Å) of $B(3)O(4)_3$ in the hexagonal tunnel is considerably shorter than the normal value (about 1.365 Å) [20], which gives rise to the significantly large BVS for B3 atom (3.816) with three-fold coordination. This could be presumably attributed to the disorder of O(4) in the tunnel because the atomic site disorder in tunnel is commonly observed in many tunnel minerals, such as apatite [21], gaudefroyite [22-23], and hollandite [24].

Lanthanide Analogues

The XRD patterns of $LiSrTb_2(BO_3)_3$ and $LiBaTb_2(BO_3)_3$ are demonstrated in Figure 2. It is evident from the simulated XRD patterns that both $LiSrTb_2(BO_3)_3$ and $LiBaTb_2(BO_3)_3$ samples are single phase. Those samples were test by the Kurtz–Perry method [25] and second harmonic generation (SHG) signal was not observed, which agrees with the former structure solution. The cell parameters of the analogues of $LiSrTb_2(BO_3)_3$ are listed in Table 4.

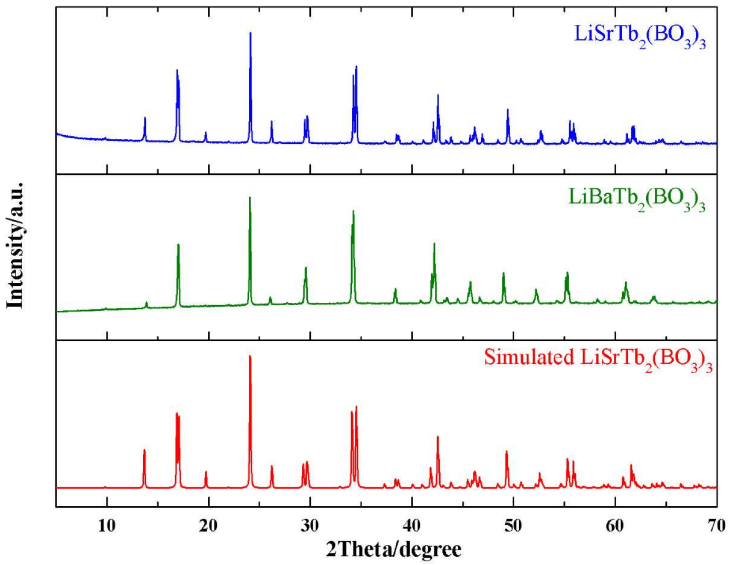

Figure 2. XRD patterns of $LiSrTb_2(BO_3)_3$ and $LiBaTb_2(BO_3)_3$

Table 4. Cell parameters for the analogues of $LiSrTb_2(BO_3)_3$

Compounds	a (Å)	c (Å)	V (Å^3)
$LiSrPr_2(BO_3)_3$	10.496	6.594	629.1
$LiSrNd_2(BO_3)_3$	10.454	6.543	619.3
$LiSrSm_2(BO_3)_3$	10.420	6.484	609.7
$LiSrEu_2(BO_3)_3$	10.421	6.474	608.8
$LiSrGd_2(BO_3)_3$	10.411	6.462	606.5
$LiSrTb_2(BO_3)_3$ [a]	10.384	6.432	600.6
$LiSrDy_2(BO_3)_3$	10.346	6.407	593.9
$LiSrHo_2(BO_3)_3$	10.327	6.391	590.2
$LiSrEr_2(BO_3)_3$	10.297	6.372	585.1
$LiSrTm_2(BO_3)_3$	10.272	6.349	580.2
$LiSrYb_2(BO_3)_3$	10.262	6.341	578.4
$LiSrLu_2(BO_3)_3$	10.230	6.318	572.7
$LiBaPr_2(BO_3)_3$	10.642	6.631	650.4
$LiBaNd_2(BO_3)_3$	10.612	6.592	642.9
$LiBaSm_2(BO_3)_3$	10.584	6.548	635.2
$LiBaEu_2(BO_3)_3$	10.558	6.494	626.9
$LiBaGd_2(BO_3)_3$	10.538	6.508	625.9
$LiBaTb_2(BO_3)_3$	10.527	6.487	622.5
$LiBaDy_2(BO_3)_3$	10.525	6.419	615.8
$LiBaHo_2(BO_3)_3$	10.444	6.481	612.3
$LiBaEr_2(BO_3)_3$	10.393	6.409	599.5
$LiBaTm_2(BO_3)_3$	10.392	6.334	592.4

a: The cell parameters of $LiSrTb_2(BO_3)_3$ are a = 10.3845(4) Å, and c = 6.4739(8) Å obtained from single crystal data.

As shown in Table 4 and the plot of unit cell parameters versus the radius of the Ln^{3+} (Figure S1), the expected trend of decreasing unit-cell volume with decreasing ionic radius is observed, which

indicates the "lanthanide contraction" takes effect. These abundant lanthanide analogues reveal that these compounds may be good phosphors or laser host lattices (Gd^{3+}or Lu^{3+}) and served as luminescent or laser materials by doping the active ions, for instance Eu^{3+} or Nd^{3+}. It should be mentioned that for Ba analogues, we are unsuccessful to prepare Yb and Lu specimens, while Tm-specimen is evidently impure. This lanthanide variation was also observed by Felsche in the course of synthesizing lanthanide silicate apatites, $Ln_{9.33}Si_6O_{26}$ [26]. Besides, attempts to isovalent substitution for $LiSrTb_2(BO_3)_3$ type such as Na^+, K^+, Mg^{2+}, Ca^{2+}, La^{3+}, Ce^{3+}, In^{3+} and Bi^{3+}, have not yet been successful.

Optical Properties

To investigate the vibration modes of the different BO_3 groups, both the IR spectrum and Raman spectrum of $LiSrTb_2(BO_3)_3$ were recorded at room temperature and given in Figure 3. The very strong (VS) bands around 1180-1300 cm^{-1} in IR spectrum and the medium strong (MS) peaks at about 1200 cm^{-1},1290 cm^{-1} in the Raman spectrum are attributed to the B-O asymmetric stretching (ν_3) of the BO_3 group [27]. The VS peak at 957 cm^{-1} in Raman and the MS peak at 938 cm^{-1} in IR can be ascribed to the symmetric stretching (ν_1) of BO_3 group, which is Raman active but IR inactive only if BO_3 group in ideal D_{3h} geometry. The appearance of the ν_1 vibration in IR further confirms the existence of distorted BO_3 groups i.e. $B(2)O_3$ in the title compound, which is highly consistent with the former structure solution. The remaining peaks around 650-770 cm^{-1} and 520-580 cm^{-1} are assigned to the out-of-plane bending (ν_2) and in-plane bending (ν_4) of BO_3 group, respectively. It should be noted that the MS peaks at 638 cm^{-1} (ν_4), 1014 cm^{-1} (ν_1) in Raman and the VS absorption at 1346 cm^{-1} (ν_3) in IR exhibit a significant "blue shift" in comparison with a normal BO_3^{3-}, which may further validate the presence of $B(3)O(4)_3$ with considerably short bond distance.

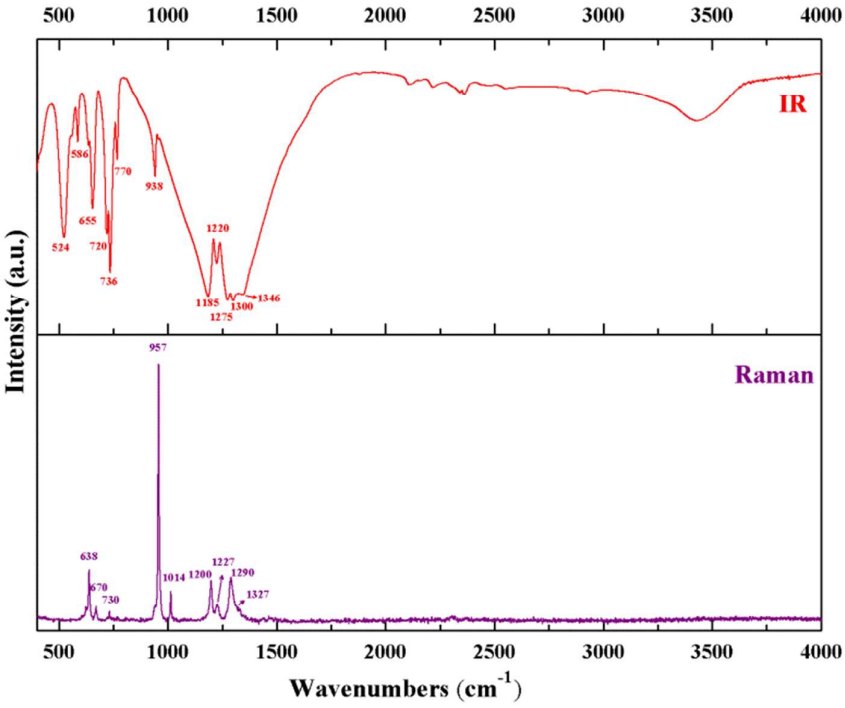

Figure 3. IR and Raman spectrum of $LiSrTb_2(BO_3)_3$

The diffuse optical reflectance spectrum of $LiSrTb_2(BO_3)_3$ measured in the range of 200–2500 nm has been converted to absorption spectrum by the Kubelka–Munk function [28] (Figure 4). According to the energy level scheme proposed by Dieke *et al* [29], the absorption peaks in the spectrum, below 400 nm, a broad band around 279 nm and an absorption peak at about 367 nm can be attributed to the $4f^8 \rightarrow 4f^7\,5d^1$ transition and $^7F_6 \rightarrow {}^5D_3$, respectively, whereas a tiny peak located at approximately 350 nm may originate from $^7F_6 \rightarrow {}^5D_2$. The visible absorption peaking at 470–500 nm may be attributed to the MO active $^7F_6 \rightarrow {}^5D_4$ transition [30], while the four peaks that may be in correspondence to $^7F_6 \rightarrow {}^7F_0$, $^7F_1$, $^7F_2$ and $^7F_3$ transitions are found in the infrared range above 1500 nm. The absorption spectrum clearly indicates that $LiSrTb_2(BO_3)_3$ is transparent in the range of 500–1500 nm.

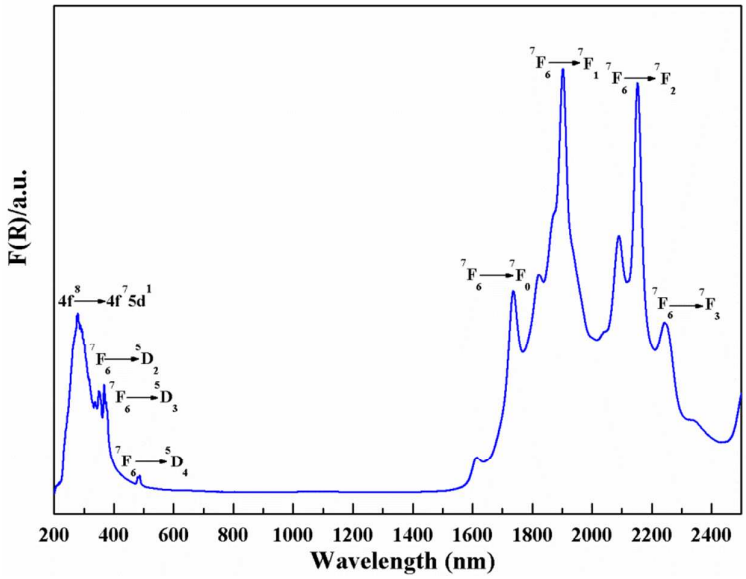

Figure 4. UV-Vis-NIR diffuse optical reflectance spectrum of $LiSrTb_2(BO_3)_3$

The fluorescence emission spectrum of $LiSrTb_2(BO_3)_3$ shows typical emission bands for Tb(III) ion when excited at 340nm (Figure 5). The strongest emission peaks are located at 540-550 nm, which is attributed to the $^5D_4 \rightarrow {}^7F_5$ transition of Tb(III) ion. The remaining emission bands can be ascribed to the transition of $^5D_4 \rightarrow {}^7F_J$ (J = 3, 4 and 6) of Tb(III) ion at 620-627 nm, 585-595 nm, 480-500 nm, respectively. The lifetimes of the Tb^{3+} ($^7F_5$) state for λ_{em}=540nm at both λ_{ex}=240 nm and 340 nm were not obtained due to the fluorescence quenching effect of the high Tb(III) concentration. [31]

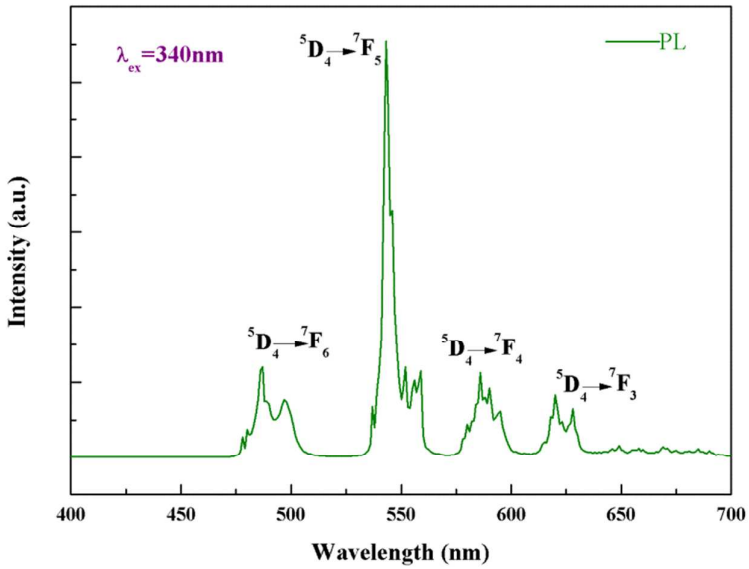

Figure 5. Fluorescence emission spectrum of $LiSrTb_2(BO_3)_3$

Thermal Analysis

It can be found that a sharp endothermic peak at 1100 °C and two strong exothermic peaks centered at around 800 °C and 555 °C in the heating and cooling curves, respectively, demonstrating that $LiSrTb_2(BO_3)_3$ may melt incongruently (Figure. 6a). To further verify the thermal behavior, $LiSrTb_2(BO_3)_3$ powder sample was sintered at 1100 °C for 2 days and then cooled to room temperature, the PXRD patterns of the thermal process residual show a mixture of $TbBO_3$ and $Sr_3Tb_2(BO_3)_4$ (Figure. 6b), which confirmed the incongruent-melting behavior of $LiSrTb_2(BO_3)_3$. Accordingly, $LiSrTb_2(BO_3)_3$ single crystals with large sizes should be grown using flux method.

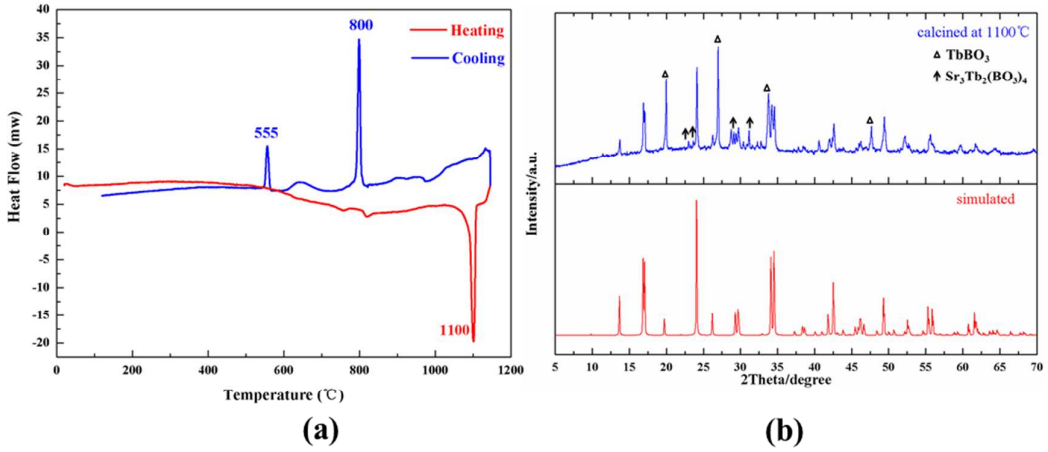

Figure 6. DSC curves for $LiSrTb_2(BO_3)_3$ (a) XRD patterns of the sample after thermal treatment under 1100 °C (b)

Magnetic Properties

The temperature-dependent magnetic susceptibilities (χ) for $LiSrTb_2(BO_3)_3$ were determined in 2−300 K temperature range at 500 Oe field. The temperature dependence of the corresponding reciprocal susceptibility (1/χ) and the molar magnetic susceptibility (χ) are displayed in Figure 7(a). $LiSrTb_2(BO_3)_3$ is found to conform to Curie–Weiss paramagnetic behaviors down to 40 K, and is fitted well with θ=-11.90K (see the red line). The effective moment μ_{eff} of Tb^{3+} ion obtained from the fitted data is 9.655(8) μ_B, which is close to the theoretical value, i.e. μ_{eff} = 9.721(1) μ_B corresponding to the ground multiplet $^7F_6$ of free Tb^{3+} ion.[32] Below 40 K, the significant deviation from the Curie–Weiss behavior is observed, implying that the single ion anisotropy of Tb(III) ion [33] may take effect. In addition, the magnetization (M) versus field isotherms at temperatures of T= 2 K in applied fields up to 9 T is exhibited in Figure 7(b). The magnetic moment for per Tb(III) ion at 9T is merely 4.66 μ_B, which does not follow the Brillouin-function and is roughly half of the theoretical Brillouin value 9 μ_B of Tb^{3+} free ion.[32] This behavior of halving the magnetization also indicates the effect from the strong single-ion anisotropy characteristic of Tb(III) ion.[34]

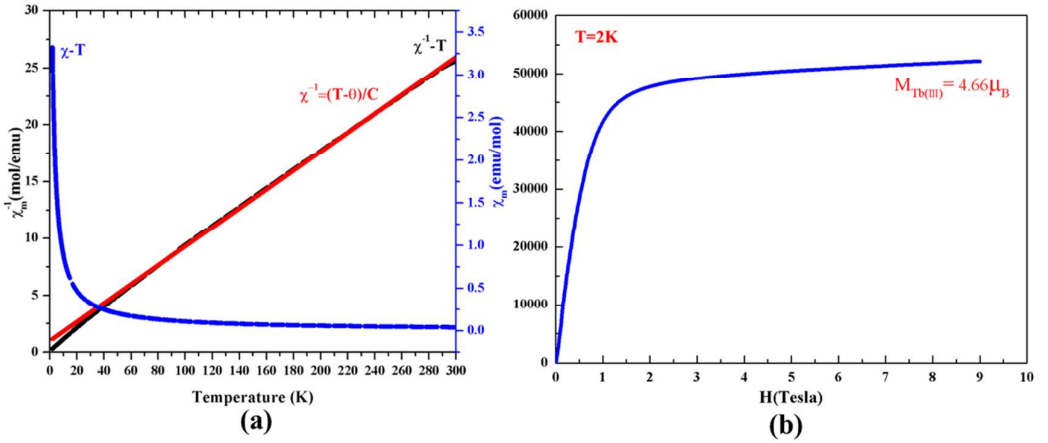

Figure 7. (a) Temperature-dependent magnetic susceptibilities of $LiSrTb_2(BO_3)_3$
(b) Magnetization isotherm for $LiSrTb_2(BO_3)_3$ at 2K up to 9T

Conclusions

A terbium rich orthoborate $LiSrTb_2(BO_3)_3$ was obtained via spontaneous crystallization, and its structure was resolved with $P\bar{3}m1$ space group by single-crystal X-ray diffraction. The isostructural analogues $LiMLn_2(BO_3)_3$ (M=Sr, Ln=Pr, Nd, Sm-Lu; M=Ba, Ln=Pr, Nd, Sm-Tm) were also prepared via solid state reaction and found to follow the lanthanide contraction. In addition, the magnetic susceptibility measurements shows that $LiSrTb_2(BO_3)_3$ exhibits paramagnetic behaviors from 300K to 2K. Owing to the trigonal symmetry, rich Tb^{3+} concentrations, and good transmittance in the range of

500-1500 nm, $LiSrTb_2(BO_3)_3$ may be a potential magneto-optical material candidate in the visible–near IR range.

Acknowledgements

This project was supported by the National Natural Science Foundation of China (Nos.90922036 and 51032004/E0201) and National Instrumentation Program (No. 2012YQ120048). P. Y. Chen is grateful to Dr. Ailin Li from Brigham Young University for bibliographic search and language help.

Notes and references

[a] *Beijing Center for Crystal Research and Development, Technical Institute of Physics and Chemistry, Chinese Academy of Sciences, Beijing 100190, P. R. China. Tel.:0086-010-82543711; E-mail: rkli@mail.ipc.ac.cn.*
[b] *University of Chinese Academy of Sciences, Beijing 100049, P. R. China*

†Electronic Supplementary Information (ESI) available: The crystallographic data for $LiSrTb_2(BO_3)_3$ has been deposited to CCDC. CCDC number is 1406528. Electronic files of the crystal structure data (CIF).

1 D. Jalas, A. Petrov, M. Eich, W. Freude, S. Fan, Z. Yu, R. Baets, M. Popović, A. Melloni, J. D. Joannopoulos, M. Vanwolleghem, C. R. Doerr, and H. Renner, Nat. Photonics, 2013, **7**, 579–582.

2 I. L. Snetkov, A. V. Voitovich, O. V. Palashov, and E. A. Khazanov, IEEE J. Quantum Electron, 2014, **50**, 434-443.

3 K. Shimamura, T. Kito, E. Castel, A. Latynina, P. Molina, E. Víllora, M. Prakasam, P. Veber, J. Chaminade, A. Funaki, T. Hatanaka, and K. Naoe, Cryst. Growth Des., 2010, **10**, 3466-3470

4 P. Veber, M. Velázquez, G.Gadret, D. Rytz, M. Peltzc, and R. Decourta, Cryst. Eng. Comm., 2015, **17**, 492-497

5 P. Chen and R. K. Li, J. Alloys Compd., 2015, **622**, 859–864

6 V. Vasyliev, E. Villora, M. Nakamura, Y. Sugahara and K. Shimamura, Opt. Express 2012, **20**, 14460-14470.

7 Z. Xia and W. Wu, Dalton Trans., 2013, **42**, 12989-12997

8 G. A. Sotiriou, D. Franco, D. Poulikakos and A. Ferrari, ACS Nano, 2012, **6**, 3888–3897

9 C. Chen, T. Sasaki, R. Li, Y. Wu, Z. Lin, Y. Mori, Z. Hu, J. Wang, S. Uda, M. Yoshimura and Y. Kaneda, Nonlinear Optical Borate Crystals, Weily-VCH, Germany, 2012.

10 X. Sun, W. Gao, T. Yang and R. Cong, Dalton Trans., 2015, **44**, 2276-2284

11 J. Chaminade, P. Gravereau, V. Jubera and C. Fouassier, J. Solid State Chem., 1999, **146**, 189-196

12 V. Jubera, P. Gravereau, J. Chaminade and C. Fouassier, J. Solid State Chem., 2001, **156**, 161-167

13 J. Lu, F. Guo and J. Chen, J. Cryst. Growth, 2011, **314**, 157–162

14 P. Thompson and D. Keszler, Solid State Ionics, 1989, **32/33**, 521-527

15 L. Song, J. Gao, X. Yang, X. Huang and G. Liu, Chinese J. Struct. Chem. 2010, **29**, 1309-1316

16 Q. Zeng and R. K. Li, Solid State Sci., 2014, **29**, 75-78

17 G. M. Sheldrick, Acta Crystallogr., Sect. A: Found. Crystallogr., 2008, **64**, 112-122.

18 G. M. Sheldrick, XPREP 6.12, SHELXTL, Bruker-AXS, 2001

19 A. Spek, J. Appl. Cryst. 2003, **36**, 7–13

20 A. F. Wells, Structural Inorganic Chemistry, fifth edition, Clarendon Press, Oxford, 1984, pp.1080

21 K. Sudarsanan, P. E. Mackie and R. A. Young, Mater. Res. Bull., 1972, **7**, 1331-1338.

22 O. Yakubovich, M. Simonov and N. Belov, Sov. Phys. Cryst., 1975, **20**, 152-155.

23 R. K. Li and C. Greaves, Phys. Rev. B, 2003, **68**, 172403

24 J. Post, R. Dreele and P. Buseck, Acta Cryst. B, 1982, **38**, 1056-1065

25 S. Kurtz and T. Perry, J. Appl. Phys., 1968, **39**, 3798–3813

26 J. Felsche, J. Solid State Chem., 1972, **5**, 266-275

27 W. Steele and J. Decius, J. Chem. Phys., 1956, **25**, 1184-1188

28 P. Kubelka and F. Munk, Tech. Phys., 1931, **12**, 593-601

29 G. Dieke and H. Crosswhite, Appl. Opt., 1963, **2**, 675-686

30 M. J. Weber, SPIE Laser and Nonlinear Optical Materials, 1986, **681**, 75-90

31 J. Feng, C. Hu, X. Xu, F. Kong and J. Mao, Inorg. Chem. 2015, **54**, 2447–2454

32 R. Carlin, Magnetochemistry, Springer-Verlag, Berlin Heidelberg, 1986

33 Y. M. Jana, O. Sakai, R. Higashinaka, H. Fukazawa, Y. Maeno, P. Dasgupta and D. Ghosh, Phys. Rev. B, 2003, **68**, 174413

34 S. Bramwell, M. Field, M. Harris and I. Parkin, J. Phys.: Condens. Matter, 2000, **12**, 483–495.

Graphic Abstract Legend

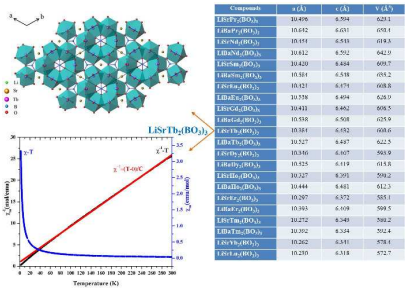

Compounds	a (Å)	c (Å)	V (Å^3)
$LiSrPr_2(BO_3)_3$	10.496	6.594	629.1
$LiBaPr_2(BO_3)_3$	10.642	6.631	650.1
$LiSrNd_2(BO_3)_3$	10.451	6.581	619.1
$LiBaNd_2(BO_3)_3$	10.612	6.592	642.9
$LiSrSm_2(BO_3)_3$	10.420	6.484	609.7
$LiBaSm_2(BO_3)_3$	10.581	6.538	635.2
$LiSrEu_2(BO_3)_3$	10.421	6.471	608.8
$LiBaEu_2(BO_3)_3$	10.578	6.494	628.9
$LiSrGd_2(BO_3)_3$	10.411	6.462	606.5
$LiBaGd_2(BO_3)_3$	10.568	6.508	629.9
$LiSrTb_2(BO_3)_3$	10.381	6.452	600.6
$LiBaTb_2(BO_3)_3$	10.527	6.487	622.5
$LiSrDy_2(BO_3)_3$	10.360	6.467	600.9
$LiBaDy_2(BO_3)_3$	10.525	6.519	625.8
$LiSrHo_2(BO_3)_3$	10.327	6.391	590.2
$LiBaHo_2(BO_3)_3$	10.444	6.481	612.3
$LiSrEr_2(BO_3)_3$	10.307	6.372	585.1
$LiBaEr_2(BO_3)_3$	10.393	6.439	569.5
$LiSrTm_2(BO_3)_3$	10.272	6.349	580.2
$LiBaTm_2(BO_3)_3$	10.392	6.384	592.4
$LiSrYb_2(BO_3)_3$	10.262	6.341	578.1
$LiSrLu_2(BO_3)_3$	10.230	6.318	572.7

A terbium rich orthoborate, $LiSrTb_2(BO_3)_3$ shows paramagnetic behaviors, and up to 21 isomorphic analogues have been prepared.